Available online at www.sciencedirect.com

ScienceDirect

www.elsevier.com/locate/jes

JES JOURNAL OF ENVIRONMENTAL SCIENCES

www.jesc.ac.cn

Identification of long-range transport pathways and potential sources of $PM_{2.5}$ and PM_{10} in Beijing from 2014 to 2015

Deping Li[1], Jianguo Liu[1,2,3], Jiaoshi Zhang[1], Huaqiao Gui[1,3,], Peng Du[1], Tongzhu Yu[1], Jie Wang[1], Yihuai Lu[1], Wenqing Liu[1,2], Yin Cheng[1]*

1. *Key Laboratory of Environmental Optics and Technology, Anhui, Institute of Optics and Fine Mechanics, Chinese Academy of Sciences, Hefei 230031, China*
2. *University of Science and Technology of China, Hefei 230026, China*
3. *Center for Excellence in Urban Atmospheric Environment, Institute of Urban Environment, Chinese Academy of Sciences, Xiamen 361021, China*

ARTICLE INFO

Article history:
Received 8 March 2016
Revised 20 June 2016
Accepted 27 June 2016
Available online 29 October 2016

Keywords:
$PM_{2.5}$
PM_{10}
Cluster analyses
PSCF
CWT
Beijing

ABSTRACT

Trajectory clustering, potential source contribution function (PSCF) and concentration-weighted trajectory (CWT) methods were applied to investigate the transport pathways and identify potential sources of $PM_{2.5}$ and PM_{10} in different seasons from June 2014 to May 2015 in Beijing. The cluster analyses showed that Beijing was affected by trajectories from the south and southeast in summer and autumn. In winter and spring, Beijing was not only affected by the trajectories from the south and southeast, but was also affected by trajectories from the north and northwest. In addition, the analyses of the pressure profile of backward trajectories showed that backward trajectories, which have important influence on Beijing, were mainly distributed above 970 hPa in summer and autumn and below 950 hPa in spring and winter. This indicates that $PM_{2.5}$ and PM_{10} were strongly affected by the near surface air masses in summer and autumn and by high altitude air masses in winter and spring. Results of PSCF and CWT analyses showed that the largest potential source areas were identified in spring, followed by winter and autumn, then summer. In addition, potential source regions of PM_{10} were similar to those of $PM_{2.5}$. There were a clear seasonal and spatial variation of the potential source areas of Beijing and the airflow in the horizontal and vertical directions. Therefore, more effective regional emission reduction measures in Beijing's surrounding provinces should be implemented to reduce emissions of regional sources in different seasons.

Introduction

Particulate matter (PM) has a significant effect on human health, visibility, direct and indirect radiative forcing, climate change and ecosystem (Andreae et al., 2008; Cao et al., 2004; Menon et al., 2002; Rosenfeld, 2000; Streets et al., 2006; Watson, 2002; Yu et al., 2014a; Yu et al., 2004; Yu et al., 2014b; Zhao et al., 2015). Pope et al. (2002) reported that 10 $\mu g/m^3$ increases in long-term average $PM_{2.5}$ ambient concentrations were associated with an almost 8% increase in the risk of lung cancer mortality. Some studies have also revealed that the increase in the daily number of deaths for all ages for a 10 $\mu g/m^3$ increase in daily PM_{10} concentrations was 0.6% (Katsouyanni et al., 2001; Krewski et al., 2003). In the most serious case, an increase of

* *Corresponding author*. E-mail: hqgui@aiofm.cn (Huaqiao Gui).

http://dx.doi.org/10.1016/j.jes.2016.06.035
1001-0742/

10 μg/m^3 of $PM_{2.5}$ results in an elevation of 4.60% and 4.48% with a lag of 3 days, values far higher than the average level of 0.69% and 1.32% for respiratory mortality and morbidity, respectively, in Beijing (Li et al., 2013).

With a rapidly developing economy, expanding anthropogenic activity and urbanization, rapid industrial growth, and an increasing number of vehicles, Beijing has suffered from heavy haze pollution in the form of PM_{10} (particulate matter, or aerosol particles, with aerodynamic diameters ≤10 μm) and $PM_{2.5}$ (diameters ≤ 2.5 μm) in recent years (Guoan et al., 2005; Ji et al., 2012; Sun, 2012; Sun et al., 2004). The average values of PM_{10} and $PM_{2.5}$ from 2004 to 2012 were 138.5 ± 92.9 and 72.3 ± 54.4 μg/m^3, respectively, in Beijing. In addition, more than 30% of days in each year exceeded the daily average PM_{10} concentration of the Grade II National Ambient Air Quality Standard (NAAQS, daily limit of 150 μg/m^3) set by the Ministry of Environmental Protection of China (Liu et al., 2015b).

The Beijing municipal government has implemented 16 rounds of air pollution control counter measures from 1998 to 2010 and a five-year clean air action plan (2013–2017) was carried out (http://www.bjepb.gov.cn/) (Wang et al., 2015b). However, the haze pollution still occurred frequently and the pollution levels remained very high (Gao et al., 2014; Liu et al., 2015a; Sun et al., 2013; Wang et al., 2014; Wang et al., 2013; Xin et al., 2016; Zhao et al., 2011a, Zhao et al., 2011b; Zheng et al., 2014). In addition, haze pollution is a regional and complex phenomenon (Hu et al., 2015; Li et al., 2012; Ren et al., 2004; Zheng et al., 2014). Regional and even super-regional pollution joint control included very effective measures of improved air quality (Chen et al., 2015b). For example, Beijing and the neighboring provinces such as Hebei, Tianjin, and Shandong implemented stringent emission control measures to ensure the air quality during the 2014 Asia-Pacific Economic Cooperation (APEC) Economic Leaders' Meetings in Beijing, 3–11 November 2014 (http://www.bjepb.gov.cn/bjepb/324122/412670/index.html, in Chinese) (Chen et al., 2015a; Meng et al., 2015). The stringent emission control measures implemented in Beijing and the regional joint control over the surroundings (especially in Hebei) were responsible for the good air quality and so-called "APEC Blue," which suggests that these measures were very effective (Li et al., 2015a; Wang et al., 2015a). However, these stringent emission control measures were present only for a temporary period and a permanent solution remains a tremendous challenge. In order to control air pollution over a sustained period, it is necessary to carry out an in-depth study of the seasonal variations in regional transport and potential source areas in Beijing.

Observation and modeling studies on regional transport and potential source areas have been introduced in previous studies in Beijing (Han et al., 2015; Li et al., 2015b; Li et al., 2015c; Wang et al., 2004, Wang et al., 2013; Wehner et al., 2002; Xia et al., 2007; Xu et al., 2008; Zhao et al., 2007; Zhu et al., 2011). However, little research has been conducted in Beijing with high temporal resolution $PM_{2.5}$ and PM_{10} data. Previous studies have only focused on PM_{10} or $PM_{2.5}$ with low temporal resolution data (6 or 24 h resolution) (Wang et al., 2015b; Zhu et al., 2011). High temporal resolution data have been shown to contribute to improved resolutions of the source areas in potential source contribution function (PSCF) calculations (Jeong et al., 2011). In addition, some studies only focused on identifying the movements of air masses in the horizontal direction (Han et al., 2015; Wang et al., 2015b; Zhu et al., 2011). To obtain comprehensive scientific analyses of the characteristics of the backward trajectory of air masses arriving in Beijing, it is essential to further study the distributions of the backward trajectory in the vertical direction.

Particulate matter is a complex media: it is composed of both primary materials emitted in the atmosphere and secondary aerosols formed in the atmosphere from various chemical processes (Wang et al., 2016). It is difficult to get the potential source regions of each particulate matter species. $PM_{2.5}$ and PM_{10} as the species of air pollution, however, the potential source regions of $PM_{2.5}$ and PM_{10} were identified by Trajectory Clustering, PSCF method and CWT method, similar previous studies (Wang et al., 2015b, Wang et al., 2006; Wang et al., 2004; Xin et al., 2016; Zhu et al., 2011). This study aims to improve understanding of the detailed transport pathways and potential sources of $PM_{2.5}$ and PM_{10} in Beijing. We identified the major air mass transport pathways in the horizontal and vertical directions using cluster analyses and the press profile of backward trajectories. And we identified the main source areas of $PM_{2.5}$ and PM_{10} in Beijing from June 2014 to May 2015, combining hourly $PM_{2.5}$ and PM_{10} concentrations using the PSCF method and the CWT method.

1. Experimental methods

1.1. Study location and monitoring data

The area of interest in this study is located in Beijing on the northern part of the North China Plain (Fig. 1a). The west of Beijing is Taihang Mountains and the north and northeast is the Yanshan Mountains. Beijing is the capital of China with a population about 21.705 million in 2015, which covers an area of 16,410.54 km^2.

The hourly $PM_{2.5}$ and PM_{10} mass concentrations for Beijing during the time period from June 1, 2014 to May 31, 2015 were obtained from the Ministry of Environmental Protection of the People's Republic of China (available at http://datacenter.mep.gov.cn/). Hourly $PM_{2.5}$ and PM_{10} concentrations were calculated by averaging concentrations from thirteen sites in Beijing (Fig. 1b). The thirteen sites included nine urban sites located in the city center (Dongsi, Guanyuan, Tiantan, Wanshouxigong, Aotizhongxin, Nongzhanguan, Gucheng, United States Embassy, Haidianwanliu), two suburban sites located in the Northwest (Dingling and Changping) and two suburban sites located in the Northeast (Huairou and Shunyi New Town).

1.2. Trajectory data

In this study, 72-hour back-trajectories arriving at the center of Beijing (116°25′29″E, 39°54′20″ N, 100 m above mean sea level) were calculated every hour (00:00–23:00 local time) using National Centers for Environmental Prediction (NCEP) reanalysis data and the Hybrid Single-Particle Lagrangian Integrated Trajectory (HYSPLIT) model version 4.9 developed by the National Oceanic and Atmospheric Administration, Air Resources Laboratory (NOAA ARL). Daily meteorological data were obtained from the global data assimilation system (GDAS) provided by NCEP, which

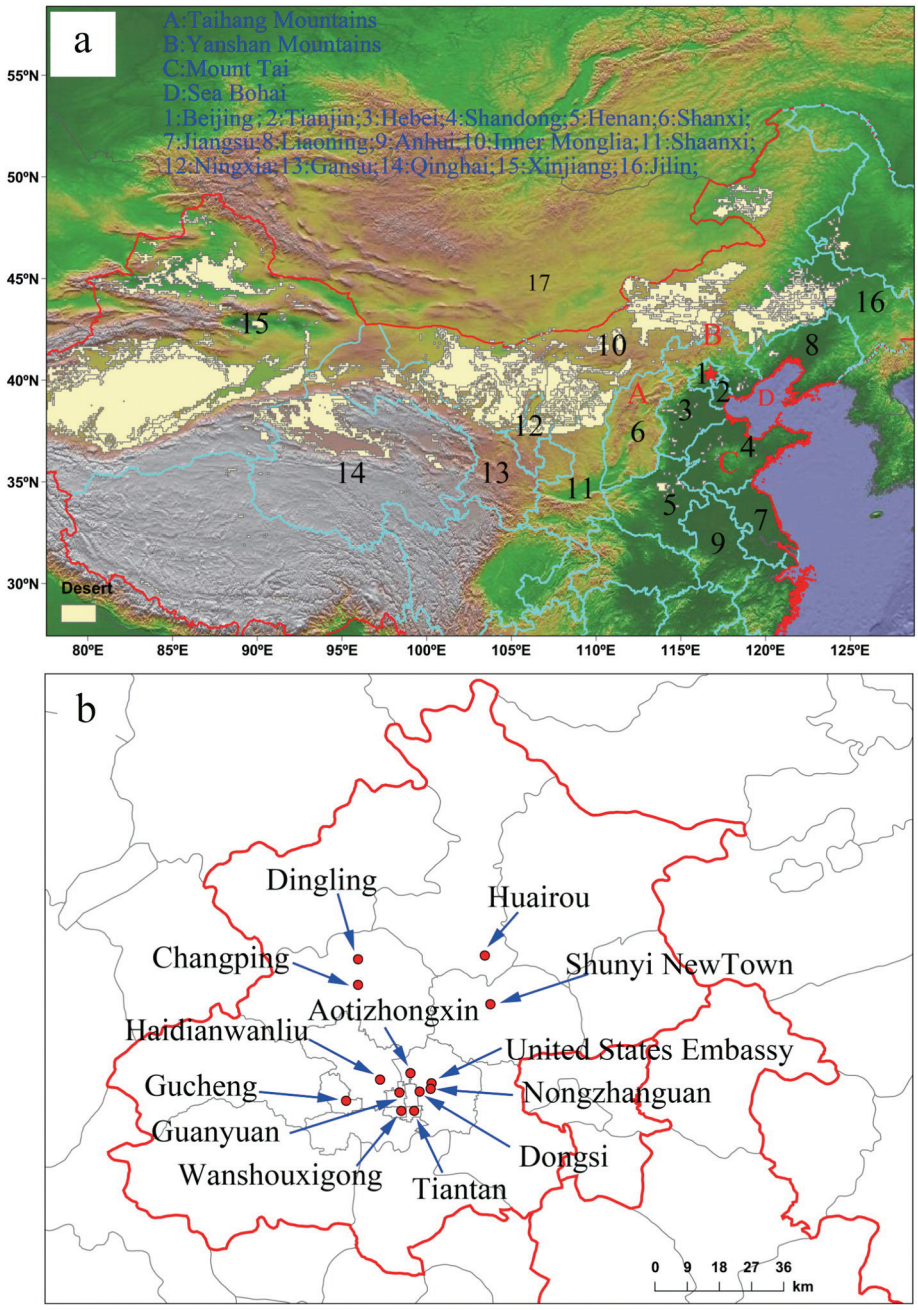

Fig. 1 – (a) Topography and location map of Beijing; (b) the distribution of the thirteen sites.

can be downloaded from the HYSPLIT website (available at ftp://arlftp.arlhq.noaa.gov/pub/archives/gdas1/).

1.3. *Trajectory clustering*

Cluster analyses, a multivariate statistical analyses technique, was used as an exploratory tool to divide the trajectory data into distinct transport groups or clusters. The trajectory cluster analysis was carried out on the basis of the GIS-based software TrajStat (Wang et al., 2009). TrajStat software has two clustering methods: Angle distance and Euclidean distance. Euclidean distance is often used to define the latitude and longitude positions as variables of the distance between two trajectories. Its main disadvantage is that if two back-trajectories have the same motion path but different speeds, they would be divided into two different categories. In the present study, we chose to use the Angle distance, not the Euclidean distance, mainly because our intention was to use the trajectories to determine the direction from which the air masses that reached the site had originated. Details of the Angle distance method are presented in Sirois and Bottenheim (1995).

1.4. *PSCF method*

The PSCF model has been widely applied to identify the possible source areas of the observed high concentrations of pollutants at the receptor site, and is a method for identifying

regional sources based on the HYSPLIT model. The ijth component of a PSCF field is defined as

$$PSCF_{ij} = \frac{x_{ij}}{y_{ij}} \quad (1)$$

where y_{ij} is the total number of trajectory endpoints that fall in the ijth grid cell and x_{ij} is the total number of trajectory endpoints for which the measured pollutant concentration exceeds a threshold value selected for this pollutant in the same grid cell (Ashbaugh et al., 1985). The pollution levels of $PM_{2.5}$ and PM_{10} were not the same in different seasons, so these values for $PM_{2.5}$ and PM_{10} were defined as the averages for different seasons during the study period, as generally used by other receptor simulation studies (Hsu et al., 2003; Wang et al., 2006). This means that the threshold value is the limit to local emissions and regional transmission. When the $PM_{2.5}$ concentration was lower than the threshold value, the $PM_{2.5}$ was contributed by the local sources. The PSCF grid covers a domain between 65 and 135°N latitude and 25–70°E longitude at 0.5 × 0.5° resolution. To remove the uncertainty in cells with small values of y_{ij}, the PSCF values were multiplied by an arbitrary weight function W_{ij} to better reflect the uncertainty in the values for these cells (Karaca et al., 2009; Polissar et al., 2001; Wang et al., 2015b; Zhu et al., 2011). The weighting function reduced the PSCF values when the total number of the endpoints in a particular cell was less than about three times the average value of the end points for each cell.

$$W_{ij} = \begin{cases} 1.0 & \left(3n_{ave} < y_{ij}\right) \\ 0.7 & \left(1.5n_{ave} < y_{ij} \le 3n_{ave}\right) \\ 0.4 & \left(n_{ave} < y_{ij} \le 1.5n_{ave}\right) \\ 0.17 & \left(y_{ij} \le n_{ave}\right) \end{cases} \quad (2)$$

1.5. CWT method

A limitation of the PSCF method is that grid cells can have the same PSCF value when sample concentrations are either only slightly higher or much higher than the criterion. As a result, it can be difficult to distinguish moderate sources from strong ones (Wang et al., 2006; Xin et al., 2016). In the CWT method, each grid cell is assigned a weighted concentration by averaging the sample concentrations that have associated trajectories that cross the grid cell, using the following equation:

$$C_{ij} = \frac{k}{\sum_{k=1}^{M} \tau_{ijk}} \sum_{k=1}^{M} C_k \tau_{ijk} \quad (3)$$

where C_{ij} is the average weighted concentration in the ijth cell, l is the index of the trajectory, M is the total number of trajectories, C_l is the concentration observed on arrival of trajectory l, and τ_{ijl} is the time spent in the ijth cell by trajectory l (Stohl, 1996; Stohl and Krompkolb, 1994; Xin et al., 2016). Like the PSCF method, CWT method also employs the arbitrary weight function to eliminate grid cells with few endpoints.

2. Results and discussion

2.1. Overview of $PM_{2.5}$ and PM_{10} concentrations

Daily mean of $PM_{2.5}$ and PM_{10} concentrations from June 1, 2014 to May 31, 2015 is displayed in Fig. 2, and the seasonal mean values of $PM_{2.5}$, PM_{10} and the ratios of $PM_{2.5}/PM_{10}$ are shown in Table 1. The annual average concentration of $PM_{2.5}$ and PM_{10} were 78.11 ± 61.08 and 114.52 ± 72.06 μg/m^3, respectively. These concentrations far exceed the limit of the Class II

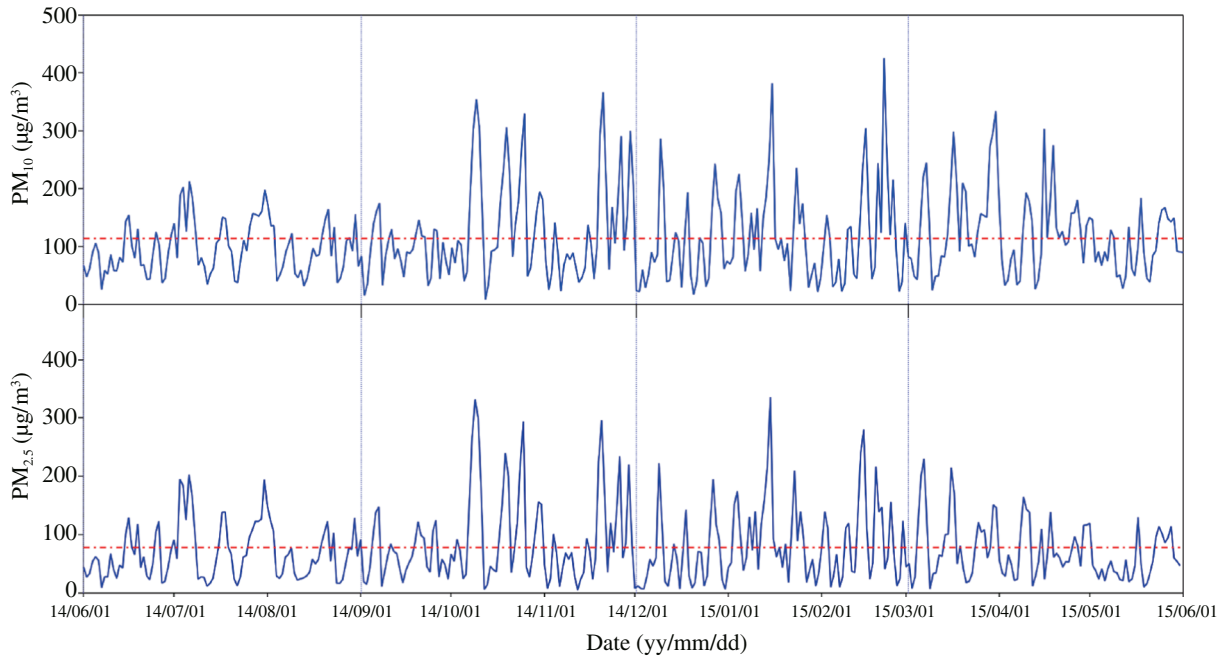

Fig. 2 – Daily means $PM_{2.5}$ and PM_{10} concentrations in Beijing, China, from June 2014 to May 2015.

Table 1 – Average $PM_{2.5}$ and PM_{10} concentrations and the ratios of $PM_{2.5}/PM_{10}$ in the four seasons.

	$PM_{2.5}(\mu g/m^3)$	$PM_{10}(\mu g/m^3)$	$PM_{2.5}/PM_{10}$
Summer	69.03 ± 46.84	96.58 ± 44.78	0.66 ± 0.19
Autumn	90.56 ± 75.39	124.64 ± 83.53	0.68 ± 0.21
Winter	82.17 ± 67.84	114.87 ± 82.36	0.67 ± 0.20
Spring	70.91 ± 48.00	122.14 ± 68.89	0.58 ± 0.20

standard of the Chinese Ambient Air Quality Standards (CAAQS, revised GB 3095-2012 of Chinese National Air Quality Standards) for $PM_{2.5}$ (limiting value of 35 $\mu g/m^3$) and for PM_{10} (limiting value of 70 $\mu g/m^3$). The ratio of $PM_{2.5}/PM_{10}$, derived from annual arithmetic means, was 0.64 ± 0.20. This result is similar to the ratio observed by previous studies (Han et al., 2010; Simonich, 2009; Wei et al., 1999; Zhang et al., 2008), indicating that $PM_{2.5}$ took a relative high portion of PM_{10}, and $PM_{2.5}$ is the major pollutant. The higher concentrations of

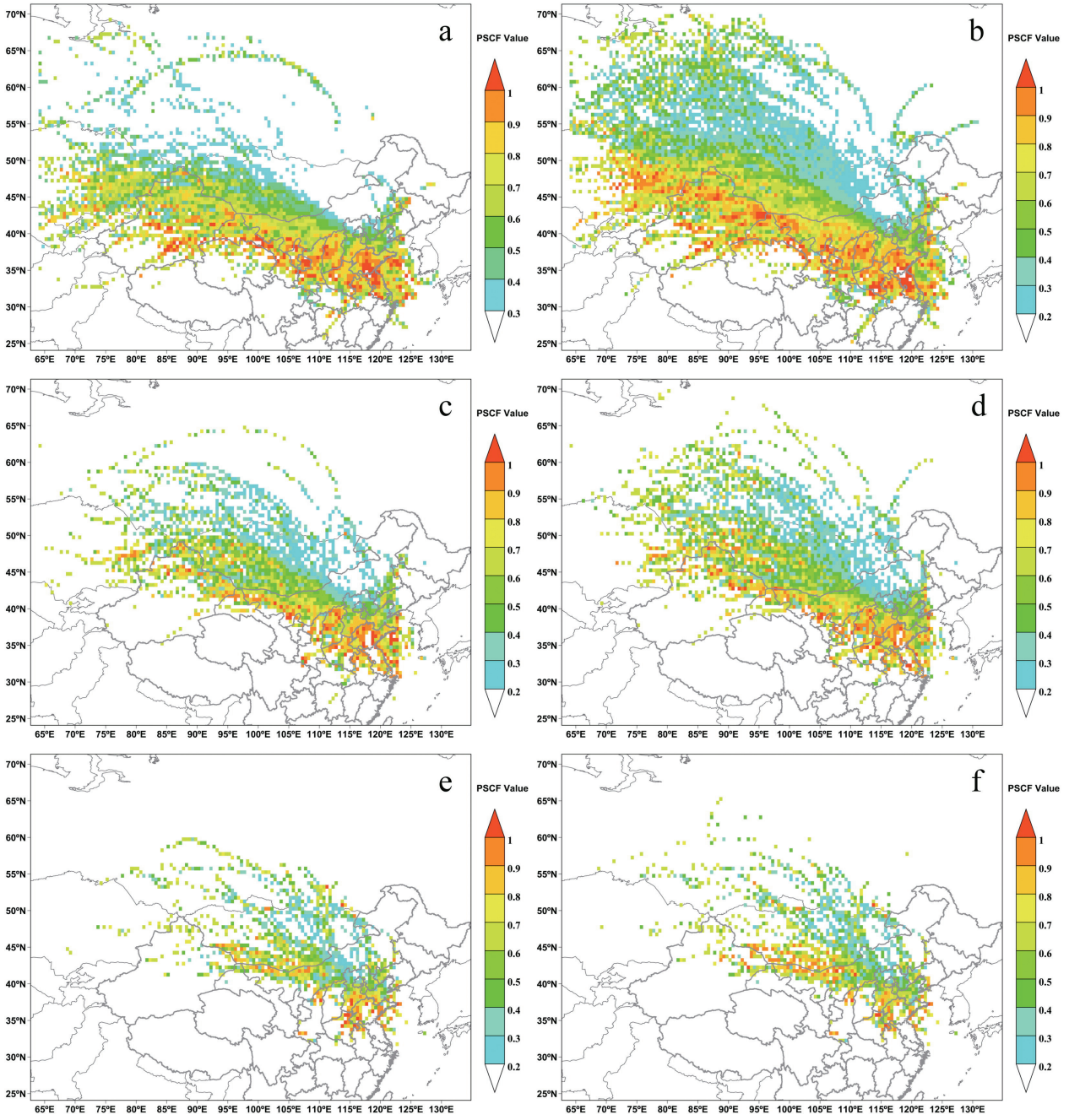

Fig. 3 – Spatial distributions of PSCF values of $PM_{2.5}$ and PM_{10} from June 2014 to May 2015. (a) $PM_{2.5}$ and (b) PM_{10} obtained *via* combining backward trajectories calculated hourly and hourly sampled data sets of each species; (c) $PM_{2.5}$ and (d) PM_{10} obtained *via* combining backward trajectories calculated every 6 hr and 6 hourly averaged data sets of each species; (e) $PM_{2.5}$ and (f) PM_{10} obtained *via* combining backward trajectories calculated every 24 j and 24 hourly averaged data sets of each species. PSCF: potential source contribution function.

$PM_{2.5}$ were mainly observed in the autumn (September, October, and November) and winter (December, January, and February); whereas, the lower concentrations were generally found in the summer (June, July, and August) and spring (March, April, and May). The higher concentrations of PM_{10} were mainly observed in the autumn, winter and spring and the lower concentrations were generally found in the summer. Seasonal variation of $PM_{2.5}$ and PM_{10} in this urban site is consistent with previous studies (Chen et al., 2015c; Sun et al., 2015; Wang et al., 2015b; Zhang et al., 2013; Zhao et al., 2009). Higher ratios of $PM_{2.5}/PM_{10}$ were mainly observed in the summer, autumn and winter, with values greater than 0.66; whereas, the lower ratios were generally found in spring, with a value of 0.58. This indicates that the coarse particles associated with the Asian dust storms were the major pollutants in spring (Jeong et al., 2011; Wang et al., 2011; Wang et al., 2004).

2.2. Sensitivity tests of time resolution of measurement samples for PSCF results

Fig. 3 shows the differences between PSCF results obtained from sampled data sets with three different time resolutions from June 2014 to May 2015. The data sets for low time resolution were obtained from averaging the hourly sampled data over every 6 hr and 24 hr. Fig. 3a,c,e shows the PSCF results obtained by combining backward trajectories and measurement of $PM_{2.5}$ in 1 hr, 6 hr and 24 hr resolution, respectively, and Fig. 3b,d,f shows the PSCF results with backward trajectory calculation and the measurements of PM_{10} in 1 hr, 6 hr and 24 hr resolution, respectively. Three different data sets revealed the different distributions of the source areas. With the improvement of time resolution, more source areas were found. This associated with more number of endpoints calculated using the HYSPLIT model and measurement data with highly temporal resolution (Jeong et al., 2011). Thus, highly time resolved data are found to contribute to better resolutions of the source areas in PSCF calculations. PSCF results obtained from using these highly time resolved input data have been also employed by the introduced algorithm to quantify the contributions of long-range transported aerosols to PM concentrations.

2.3. Cluster analyses

Six main trajectory clusters were divided according to the coherence of the characteristics of spatial distribution of each trajectory using HYSPLIT model (Fig. 4). The six clusters and their corresponding $PM_{2.5}$ and PM_{10} concentrations are described in Figs. 5 and 6. Table 2 shows the number of trajectories assigned to each cluster, the mean $PM_{2.5}$ and PM_{10} concentrations and the ratios of $PM_{2.5}/PM_{10}$ for each cluster.

In summer, ratios of $PM_{2.5}/PM_{10}$ for Clusters 1, 3 and 6 were 0.81, 0.71 and 0.78, respectively. However, the ratios of $PM_{2.5}/PM_{10}$ for the Clusters 2, 4, and 5 were considerably lower at 0.45, 0.44, and 0.55, respectively. The air masses of Clusters 1, 3, and 6 were considered to be the major pollutant

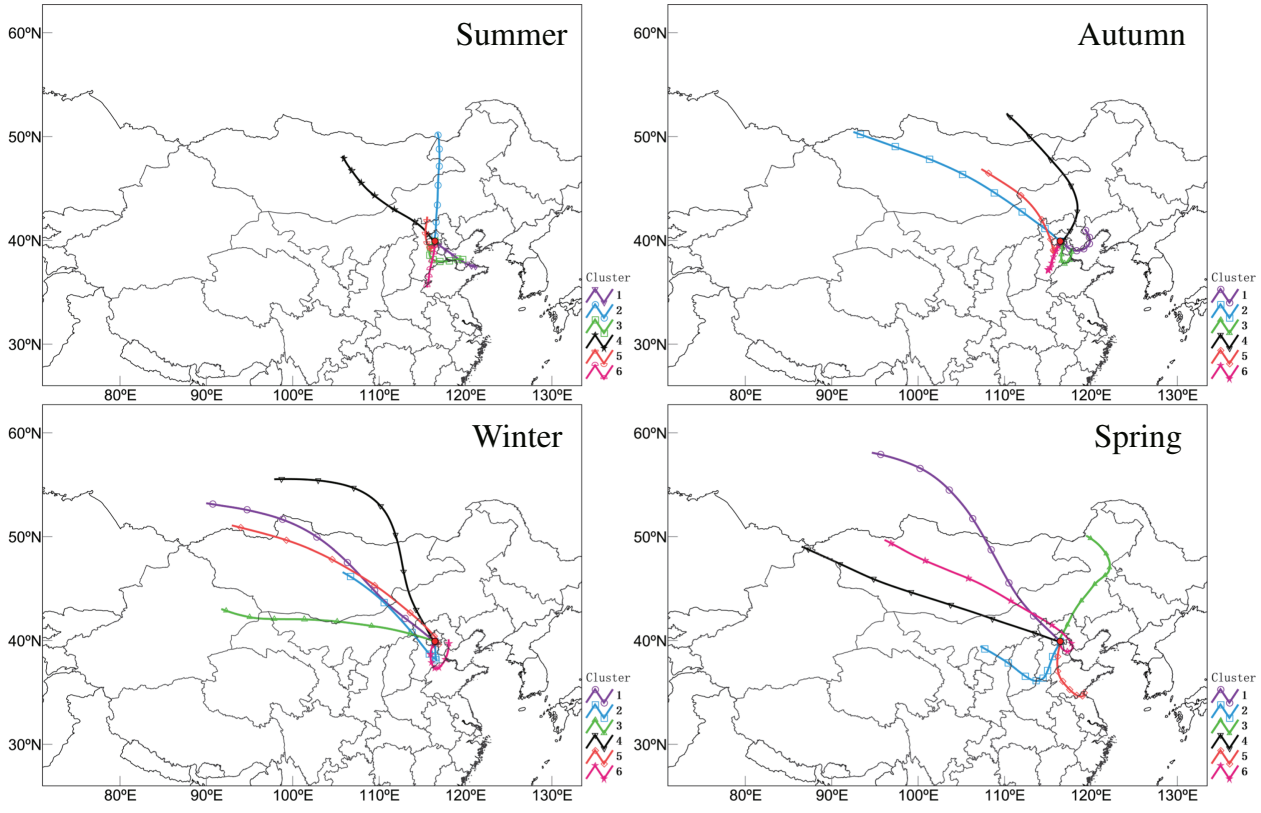

Fig. 4 – Cluster-mean back-trajectories in Beijing from June 2014 to May 2015.

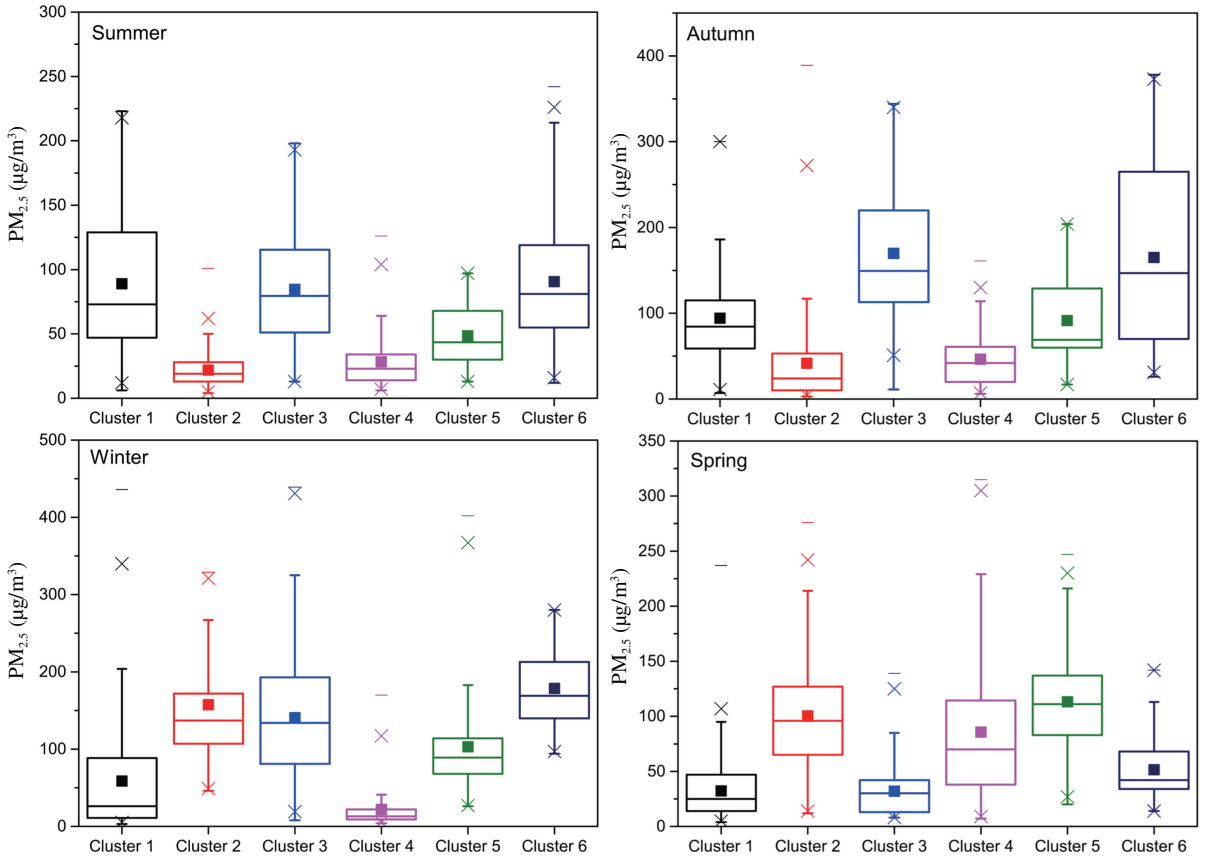

Fig. 5 – Box plots of $PM_{2.5}$ associated with the six trajectory clusters on a seasonal basis. The box-charts show $PM_{2.5}$ mean values, together with the maximum, the minimum, and the 95th, 75th, 50th, 25th, and 5th percentiles.

trajectories because these clusters were associated with $PM_{2.5}$ and PM_{10} concentrations higher than the average concentration of summer (Table 1). Mean $PM_{2.5}$ loadings associated with Clusters 1, 3 and 6 were the highest of all clusters at 88.97, 84.68 and 90.65 μg/m^3, respectively. Mean PM_{10} loadings associated with Clusters 1, 3 and 6, were 108.62, 119.32 and 115.59 μg/m^3, respectively (Table 1). High numbers of polluted trajectories were assigned to Clusters 1, 3 and 6. In contrast, Clusters 2, 4 and 5 were considered less important as pathways for pollutants. The air masses associated with Clusters 1, 3 and 6 accounted for about 64.48% of all trajectories and started from south and southeast and went through northern Shandong, southern central of Hebei and Tianjin which were the developed industrial areas. The air masses associated with Clusters 2, 4 and 5 started from north and northwest and passed through the center of Mongolia and Inner Mongolia, and northern Hebei. Therefore, Beijing always has the highest ratios of $PM_{2.5}/PM_{10}$ when the air mass came from south and southeast, and passed through areas associated with anthropogenic aerosol emissions and has the lowest ratios of $PM_{2.5}/PM_{10}$ when the air mass came from the north and northwest.

In autumn, ratios of $PM_{2.5}/PM_{10}$ for Clusters 1, 3, 5 and 6 were 0.79, 0.81, 0.65, and 0.79, respectively. The ratios of $PM_{2.5}/PM_{10}$ for Clusters 2 and 4 were 0.56 (Table 2). The air masses of Clusters 1, 3, 5 and 6 were regarded as the major polluted trajectories contributing to $PM_{2.5}$ and PM_{10} in Beijing. This is because air masses of Clusters 1, 3, 5 and 6 are associated with concentrations of $PM_{2.5}$ and PM_{10} that were higher than the average concentration in autumn (Table 1). Of these four major pathways, Clusters 3 and 6 are the most important air masses because they have the highest mean $PM_{2.5}$ (169.78 and 165.17 μg/m^3) and PM_{10} (208.47 and 209.05 μg/m^3) concentrations and a large number of polluted trajectories (Table 2). The air masses associated with Clusters 3 and 6 started from the south and southeast and passed through northwest Shandong and southeast Hebei and onwards to Beijing. The air masses associated with Clusters 2 and 5 started from the north and northwest and passed through areas associated with natural aerosol emissions.

In winter, the ratios of $PM_{2.5}/PM_{10}$ for Clusters 2, 3, 5 and 6 were 0.84, 0.82, 0.73, and 0.80, respectively. The ratios of $PM_{2.5}/PM_{10}$ for Clusters 1 and 4 were 0.62 and 0.47, respectively. The air masses associated with Clusters 2, 3, 5 and 6, accounting for about 39% of all trajectories, may be considered the main air masses which have a significant influence on $PM_{2.5}$ and PM_{10} concentrations. Because these air masses have the highest mean $PM_{2.5}$ and PM_{10} concentrations. Cluster 2 came from the northwest and passed through northeast Shanxi and southern Hebei. Cluster 3 started from Xinjiang and passed through Inner Mongolia, northeast Shanxi, and northwest Hebei. Clusters 1, 4, and 5 started from Russia and passed through Mongolia, Inner Mongolia, and north Hebei. Cluster 5 was different from Clusters 1 and 4, because it passed through Beijing to northern

Tianjin and then turned back to Beijing. Cluster 6 started from northeast Hebei and passed through northwest Shandong and southern Hebei.

In spring, the ratios of $PM_{2.5}/PM_{10}$ were lower than other seasons, at 0.38 to 0.7. The ratios of $PM_{2.5}/PM_{10}$ of Clusters 2, 4 and 5 were 0.6, 0.6, and 0.7, respectively. Their masses associated with Clusters 2, 4 and 5, accounted for about 62.8% of all trajectories and may be considered important pathways with high $PM_{2.5}$ and PM_{10} concentrations. Cluster 2 came from southern Inner Mongolia and passed through Shanxi, northern Henan, and southern Hebei. Cluster 4 which was similar to the transport pathways of sand storms discussed by Wang et al. (2004), came from northern Xinjiang and passed through desert and semi-desert regions in southwestern Mongolia, and then through the middle of Inner Mongolia and onwards to Beijing. Cluster 5 started from north Jiangsu and passed through Shandong and southern Hebei. The air masses associated with Cluster 6, accounting for about 4.8% of all trajectories, represented pathway polluted by PM_{10} but not $PM_{2.5}$. The air masses associated with Cluster 6 that started from northwest Mongolia, went through the central of Mongolia and Inner Mongolia, northern Hebei, and Tianjin before reaching Beijing. Therefore, the air masses associated with Cluster 6 were the transport pathways of sand storms, which were consistent with previous studies (Zhang et al., 2012; Zhang et al., 2010).

Generally speaking, polluted trajectories always had high ratios of $PM_{2.5}/PM_{10}$ (≥0.65) in summer, autumn and winter, which indicated that the regional transport had an important impact on $PM_{2.5}$ in Beijing. In spring, Beijing was affected by Asian dust, so polluted trajectories had the low ratios of $PM_{2.5}/PM_{10}$. The number of $PM_{2.5}$ and PM_{10} polluted trajectories were 36.98%, 34.16%, 38.65% and 41.73% of total trajectories in summer, autumn, winter and spring, respectively. This is similar to the conclusions of Lv et al. (2015). Beijing is easily affected by trajectories from the south and southeast in summer and autumn; however, in winter and spring. Beijing is not only affected by the trajectories from the south and southeast, but also by trajectories from the north and northwest.

2.4. *Pressure profiles of backward trajectories*

To obtain comprehensive scientific analyses of the characteristics of backward trajectories arriving in Beijing, it is essential to further study the distributions of backward trajectories in the vertical direction. As shown in Fig. 7, pressure profiles backward trajectory analyses found clear differences in the distributions of backward trajectories arriving in Beijing in the vertical direction. The mean and standard deviation of barometric altitude for every cluster in every season is shown in Table 3.

There was a significant difference in the path of air masses in the vertical direction in summer. At 975 hPa barometric altitude (344 m), air masses associated with Clusters 2 (857.20 hPa), 4 (781.63 hPa) and 5 (936.10 hPa), with corresponding heights of

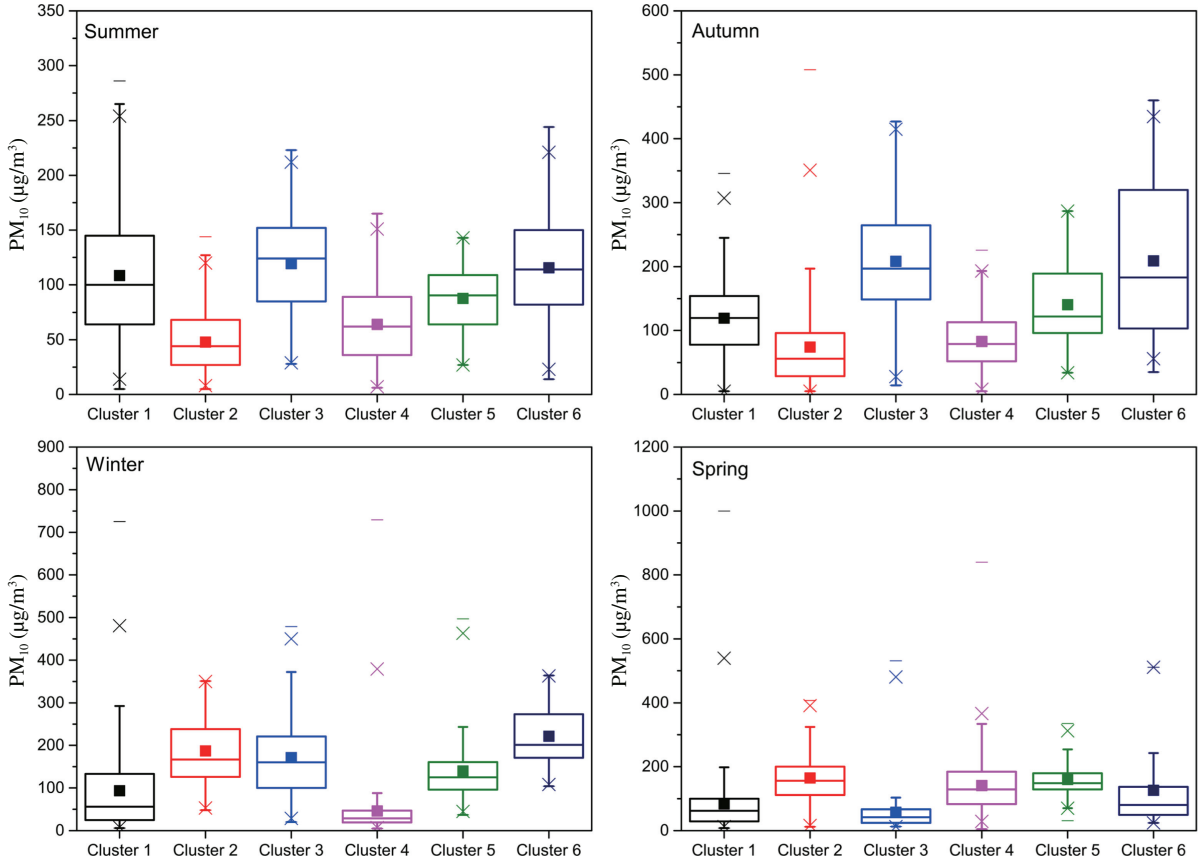

Fig. 6 – Box plots of PM_{10} associated with the six trajectory clusters on a seasonal basis. The box-charts show PM_{10} mean values, together with the maximum, the minimum, and the 95th, 75th, 50th, 25th, and 5th percentiles.

Table 2 – Trajectory numbers and $PM_{2.5}$, PM_{10} mean concentrations and the $PM_{2.5}/PM_{10}$ ratios for each cluster.

	Clusters	NAL [a]	PAL [b](%)	$PM_{2.5}$(μg/m^3)	PM_{10}(μg/m^3)	NPL1 [c]	NPL2 [d]	$PM_{2.5}/PM_{10}$
Summer	1	706	32.19	88.97	108.62	349	302	0.81
	2	396	18.06	21.88	47.80	3	15	0.45
	3	162	7.39	84.68	119.32	84	98	0.71
	4	258	11.76	28.27	63.95	11	55	0.44
	5	103	4.70	48.51	87.78	23	37	0.55
	6	568	25.9	90.65	115.58	304	304	0.78
Autumn	1	366	16.76	94.19	119.19	147	141	0.79
	2	788	36.08	41.64	74.20	84	122	0.56
	3	291	13.32	169.78	208.47	219	193	0.81
	4	279	12.77	46.56	83.02	29	45	0.56
	5	125	5.72	91.59	140.4	36	44	0.65
	6	335	15.34	165.17	209.05	189	201	0.79
Winter	1	775	36.18	58.65	93.38	188	218	0.62
	2	157	7.33	157.56	187.26	130	115	0.84
	3	424	19.79	140.83	171.19	290	255	0.82
	4	505	23.58	21.89	46.15	17	23	0.47
	5	163	7.61	103.07	140.03	86	88	0.73
	6	118	5.51	178.64	221.48	117	103	0.80
Spring	1	522	24.45	32.33	83.4	40	88	0.38
	2	260	12.18	100.40	164.64	180	170	0.60
	3	145	6.79	32.07	57.31	10	3	0.55
	4	801	37.52	85.66	140.81	350	372	0.60
	5	305	14.29	113.17	159.88	243	224	0.70
	6	102	4.78	51.48	126.01	21	34	0.40

[a] NAL is the number of all trajectories.
[b] PAL is the percentage of all trajectories (%).
[c] NPL1 is the number of trajectories associated with concentration higher than the average concentration of every season for $PM_{2.5}$. The average concentrations of every season for $PM_{2.5}$ are presented in Table 1.
[d] NPL2 is the number of trajectories associated with concentration higher than the average concentration of every season for PM_{10}. The average concentrations of every season for PM_{10} are presented in Table 1.

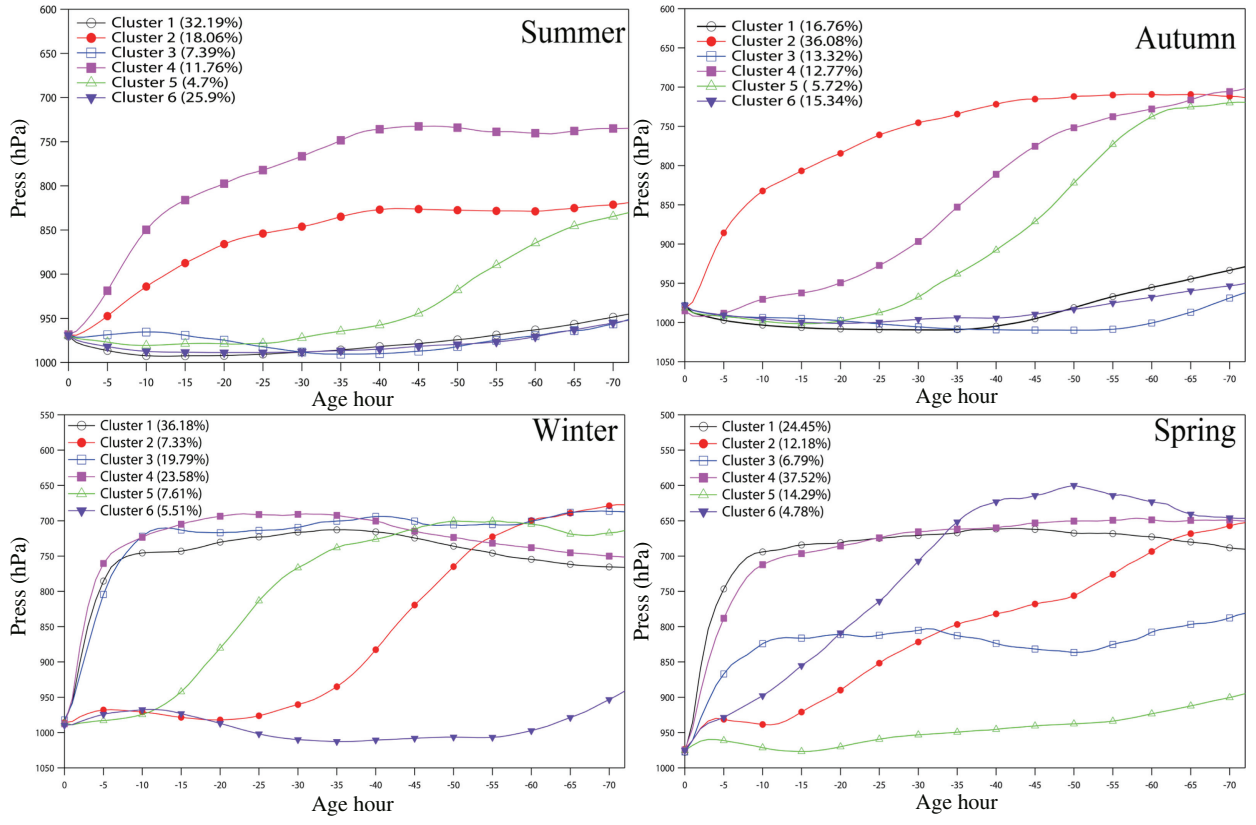

Fig. 7 – The pressure profile of backward trajectories from June 1, 2014 to May 31, 2015 in Beijing.

Table 3 – The mean and standard deviation of barometric altitude for every cluster in different season (hPa).

	Summer	Autumn	Winter	Spring
Cluster 1	978.40 ± 114.55	987.30 ± 117.49	749.29 ± 99.37	690.43 ± 97.09
Cluster 2	857.20 ± 108.64	762.18 ± 112.09	864.37 ± 156.17	806.71 ± 134.41
Cluster 3	975.69 ± 113.9	998.32 ± 116.62	722.31 ± 101.60	824.58 ± 101.72
Cluster 4	781.63 ± 111.54	846.97 ± 143.54	728.55 ± 98.96	685.93 ± 102.94
Cluster 5	936.10 ± 120.38	892.54 ± 149.16	799.40 ± 142.93	946.29 ± 112.17
Cluster 6	979.81 ± 114.34	985.46 ± 115.51	991.81 ± 116.77	722.64 ± 146.55

about 1404, 2084 and 694 m, respectively, came from the north and had long pathways and through clean areas (Fig. 4). This therefore reduced the pollution in Beijing. At 975 hPa heights, air masses associated with Clusters 1 (978.40 hPa), 3 (975.69 hPa) and 6 (979.81 hPa) were the most important back-trajectories in terms of their influence on Beijing City. Those clusters mainly came from south, had short transport pathways, and passed through the industrially developed areas in Shandong and Hebei. These air masses carried pollutants to Beijing, which increased the pollution in Beijing itself as showed in the above analyses. In autumn, Clusters 1, 3 and 6 may be regarded as the major polluted trajectories contributing to $PM_{2.5}$ and PM_{10} in Beijing below 985 hPa (about 254 m). These clusters came from the south and passed through industrially developed areas in Hebei and Tianjin, thus transporting anthropogenic contaminants to Beijing. In winter, the air masses associated with Clusters 2 and 5 came from the northwest. Blocked by high mountains, those two air masses traveled in an arc through industrially developed areas in Hebei and carried anthropogenic contaminants to Beijing. Cluster 3, above 750 hPa heights (about 2400 m), was considered as important pathway because this cluster was mainly from Xinjiang and passed through desert and semi-desert regions in the middle of Inner Mongolia and onwards to Beijing carrying natural dust. Cluster 6 (991.81 hPa; about 192 m), included the air masses polluted by anthropogenic contaminants that originated from the south and passed

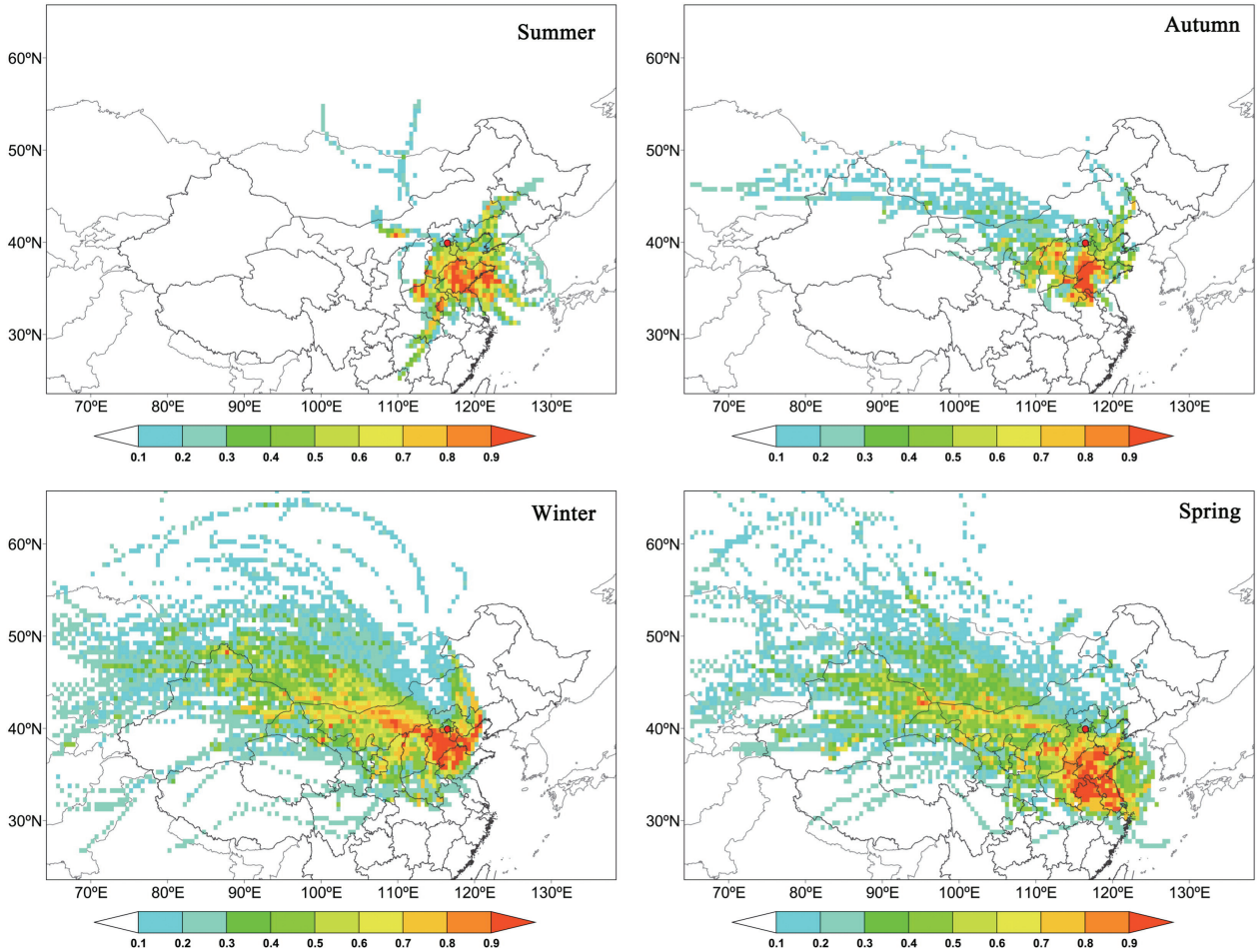

Fig. 8 – WPSCF maps for Beijing $PM_{2.5}$ in summer, autumn, winter and spring from June 1, 2014 to May 31, 2015. WPSCF: Weighted Potential Source Contribution Function.777

through industrially developed areas in Hebei. In spring, the air masses associated with Cluster 4 were considered the most important back-trajectory above 750 hPa (2400 m) barometric altitude. This cluster was mainly from Kazakhstan and passed through desert and semi-desert regions in southwestern Mongolia, and then through the middle of Inner Mongolia and onwards to Beijing, similar to the "Northerly Mongolia Path" identified by Wang et al. (2004). Clusters 2 and 5 (height of about 600–1800 m) may be considered the air masses polluted by anthropogenic contaminants that came from the south and southwest, and passed through industrially developed areas in Shanxi, Shandong and Hebei.

Overall, in summer and autumn, Beijing was mainly influenced by airflows that were distributed above 970 hPa barometric altitude. This indicated that the near surface air masses had important influence on $PM_{2.5}$ and PM_{10} concentrations. Such airflows had short transport pathways passing through the areas associated with anthropogenic pollutants, such as Shandong, Hebei, and Tianjin. In winter and spring, Beijing was mainly influenced by airflows at 950 hPa barometric altitude. These airflows had long transport pathways passing through the desert and semi-desert regions. This indicates that high altitude air masses had an important influence on $PM_{2.5}$ and PM_{10} concentrations in winter and spring.

2.5. PSCF and CWT analyses

Cluster analyses provide a useful tool for studying transport pathways of pollutants and identifying the potential transport source areas to Beijing (Xin et al., 2016). However, it has some parameters which are regarded as subjective, such as the selections of the clustering algorithm, number of clusters and the distance definition (Wang et al., 2009). Furthermore, it cannot simulate the values of $PM_{2.5}$ and PM_{10} levels caused by potential source areas. To obtain a better understanding of long-range transport that may have an important influence on $PM_{2.5}$ and PM_{10} levels in Beijing and to find potential source areas, further study was needed to analyze the potential sources with PSCF and CWT methods.

The WPSCF (Weighted Potential Source Contribution Function) results describe the spatial distributions of $PM_{2.5}$ potential sources obtained by combining backward trajectories and measurements of $PM_{2.5}$ and are shown in Fig. 8. The colors represent the contribution levels of potential source area and the red color could be associated with high concentrations while the blue color represents low $PM_{2.5}$ concentrations. The WPSCF map distributions for different seasons were significantly different because of the differences in the air flows in different seasons. It could be seen that high WPSCF values were found in the Shandong Peninsula, the

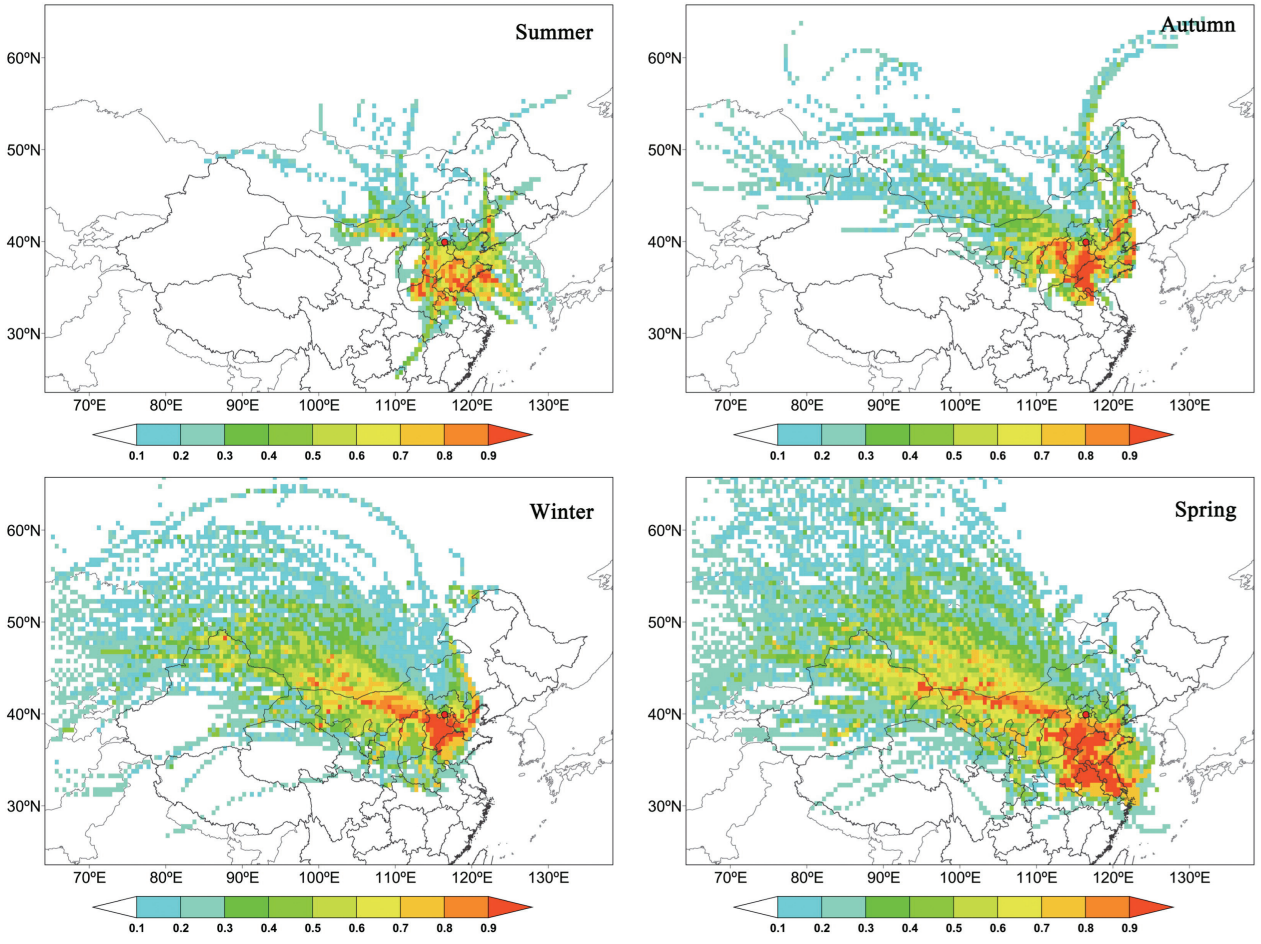

Fig. 9 – WPSCF maps for Beijing PM_{10} in summer, autumn, winter and spring from June 1, 2014 to May 31, 2015.

south region of Hebei, north Henan and northeast Shanxi in Fig. 8a,b. Therefore those places could be considered as the main potential source area in summer and autumn. In winter and spring, high WPSCF values were found in southern of Hebei, eastern of Henan, northern of Shanxi, Shandong, northern of Jiangsu and Anhui, and the farther Mongolia, Xinjiang, Inner Mongolia and Shaanxi area.

Fig. 10 shows the PSCF maps of the potential sources of $PM_{2.5}$ in Beijing during 2005–2010 which were analyzed by Wang et al. (2015b) with 6 hour resolution data. By comparing Figs. 8 and 10, it could be found that more potential source areas could be found with the high resolution data, such as Mongolia, Xinjiang in winter and spring. So highly time resolved data are found to contribute to better resolutions of the source areas in PSCF calculations.

Fig. 9 shows the map of Beijing PM_{10} in different seasons using the PSCF method. The largest potential source areas of PM_{10} were found in spring, followed by winter and autumn, then summer. Comparing the two maps of PM_{10} and $PM_{2.5}$, it could be found that the potential source regions of PM_{10} were similar to $PM_{2.5}$. However, the southwest of Liaoning and the Bohai Sea also were the potential source areas of PM_{10} in autumn.

The results of $PM_{2.5}$ concentrations identified by the CWT method (Fig. 11) were very similar to the results found using the PSCF method. The regions with red color corresponded to the main contributing sources associated with the highest $PM_{2.5}$ values. In summer, the highest WCWT (Weighted Concentration-Weighted Trajectory) values covering the map were distributed in Shandong Peninsula, the south region of Hebei, the border of Henan, Anhui and Jiangsu. These areas were the main contributing sources to the highest $PM_{2.5}$ values (far exceeding 100 $\mu g/m^3$). In autumn, the highest WCWT values covering the map were distributed in the west of Shandong, the south region of Hebei, and the border of Henan, Anhui and Jiangsu. Those areas were the main contribution sources associated with the highest $PM_{2.5}$ concentrations of 130 $\mu g/m^3$. In winter, the high WCWT values were mainly located in the northwest of Shandong, the south of Hebei, the northeast of Shanxi and the middle

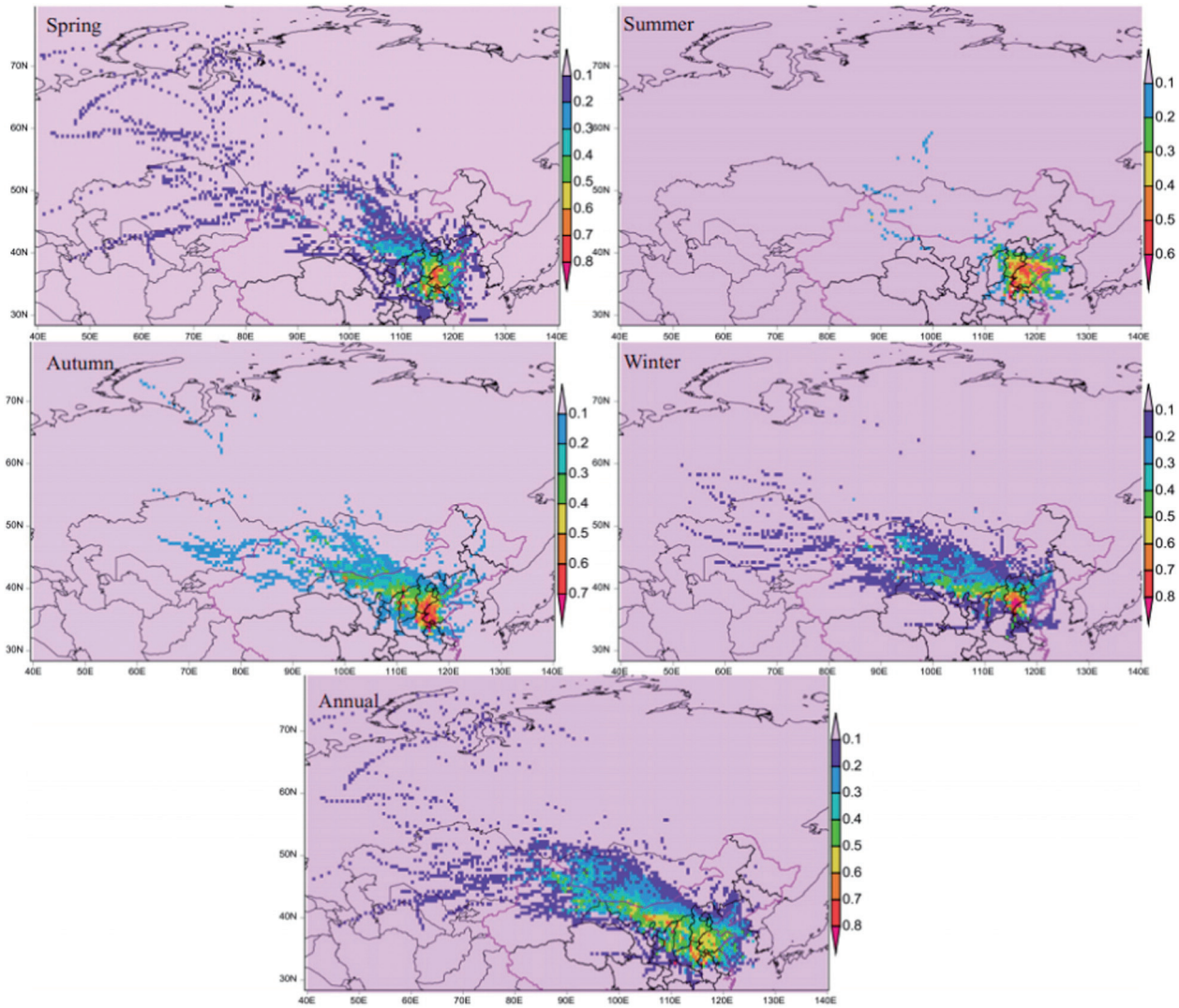

Fig. 10 – The PSCF maps of the potential sources of $PM_{2.5}$ in Beijing during 2005–2010 with 6 hr resolution data ((Wang et al., 2015b)). PSCF: potential source contribution function.

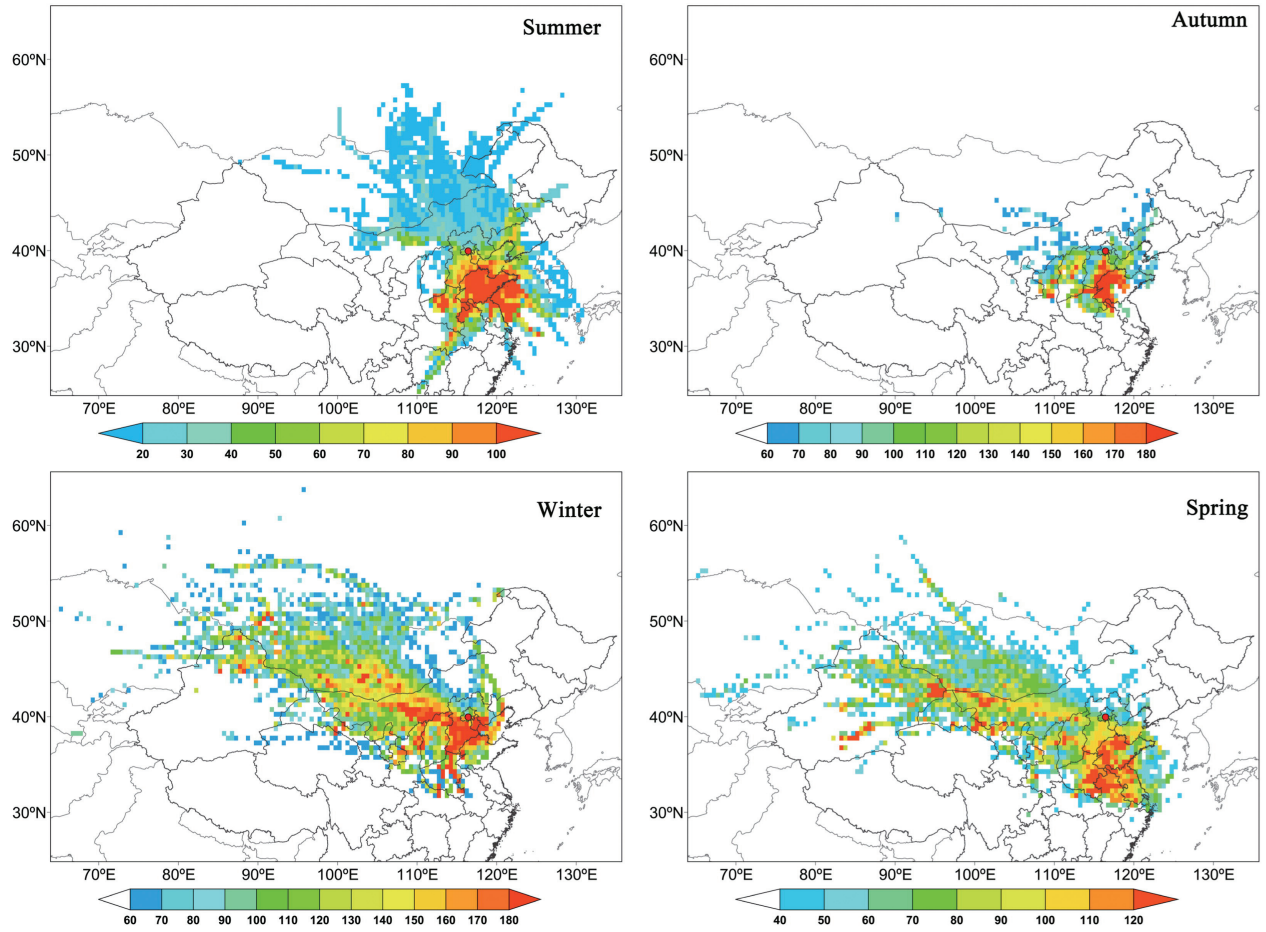

Fig. 11 – WCWT maps for Beijing $PM_{2.5}$ in summer, autumn, winter and spring from June 1, 2014 to May 31, 2015. WCWT: Weighted Potential Source Contribution Function.

of Inner Mongolia with the high WCWT values were about 100–180 μg/m^3. In spring, the highest WCWT values in the map were distributed in Jiangsu, northern Anhui, Shandong province, northeast Henan, eastern Shanxi, southern Hebei, Inner Mongolia and south Mongolia with the highest WCWT values at about 80–180 μg/m^3.

Fig. 12 shows the distributions of weighted trajectory concentration of PM_{10}. Comparing Figs. 11 and 10, we found that the WCWT map of PM_{10} was very similar to the WCWT map of $PM_{2.5}$. The potential source areas associated with the high WCWT values for PM_{10} were about 70–100, 120–200, 120–180 and 120–180 μg/m^3 in summer, autumn, winter and spring, respectively.

3. Conclusions

In this study, cluster analyses was applied to identify the main trajectory groups in the horizontal direction and the origins and distributions of major trajectory groups in the vertical direction with high resolution data from June 2014 to May 2015 in Beijing, China. The PSCF CWT models were applied to identify the major potential source areas. The statistical results of $PM_{2.5}$ and PM_{10} suggested that the annual average concentrations of $PM_{2.5}$ and PM_{10} were 78.11 ± 61.09 μg/m^3 and 114.53 ± 72.07 μg/m^3, respectively. The ratios of $PM_{2.5}/PM_{10}$ were 0.66 ± 0.19, 0.68 ± 0.21, 0.67 ± 0.2 and 0.58 ± 0.2 in summer, autumn, winter and spring, respectively. These indicated that $PM_{2.5}$ is the dominant pollutant. Six major trajectory pathways were identified using trajectory cluster analyses. The number of trajectories polluted by $PM_{2.5}$ and PM_{10} were 36.98%, 34.16%, 38.65% and 41.73% in summer, autumn, winter and spring, respectively.

The polluted trajectories always had high ratios of $PM_{2.5}/PM_{10}$ (≥0.65) in summer, autumn and winter, which indicated that the regional transport had an important impact on $PM_{2.5}$ in Beijing. Beijing was affected by trajectories from the south and southeast in summer and autumn. However, in winter and spring, Beijing was not only affected by the trajectories from south and southeast, but also by trajectories from the north and northwest. In addition, the results of the pressure profile of the backward trajectories showed that the backward trajectories with the most important influence were mainly distributed above 970 hPa in summer and autumn and below 950 hPa in spring and winter. This indicates that the near surface air mass had important influences on $PM_{2.5}$ and PM_{10} in summer and autumn and high altitude air masses had important influences on $PM_{2.5}$ and PM_{10} in winter and spring.

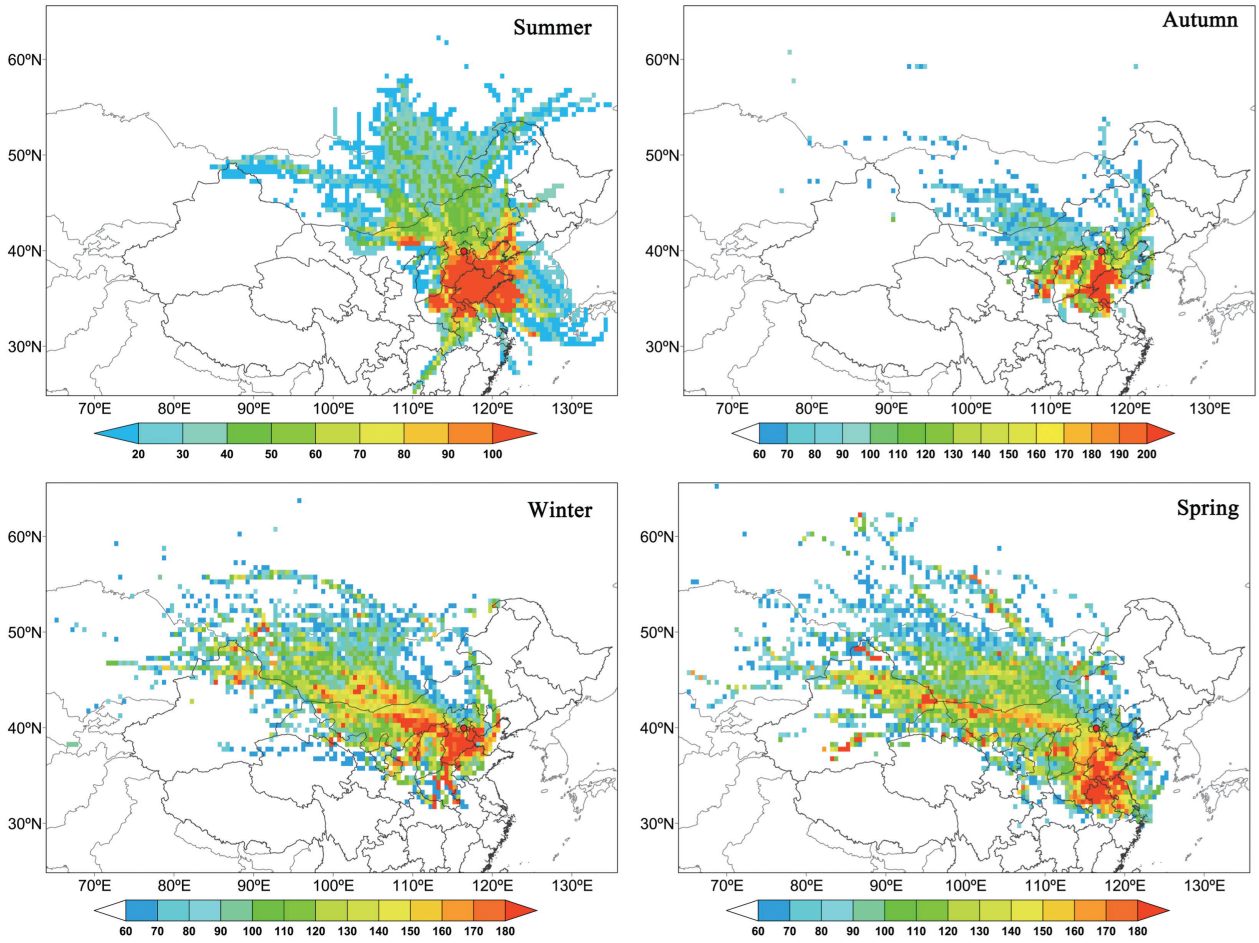

Fig. 12 – WCWT maps for Beijing PM_{10} in summer, autumn, winter and spring from June 1, 2014 to May 31, 2015. WCWT: Weighted Potential Source Contribution Function.

The PSCF and CWT methods were applied to identify the $PM_{2.5}$ and PM_{10} levels and potential source areas. The results showed that the largest potential sources occurred in spring, followed by winter and autumn, then summer. And the potential source regions of PM_{10} were similar to those of $PM_{2.5}$. However, the center of Inner Mongolia had a higher WPSCF value for PM_{10} than for $PM_{2.5}$ in spring. This was related to the dust storms in spring. In summer and autumn, the potential source areas were located in the Shandong Peninsula, south of Hebei, northeast of Shanxi, northeast Hebei and the north Henan, and contributed to high PM loadings in Beijing. These areas contributed $PM_{2.5}$ concentrations from 90 to 180 $\mu g/m^3$ and PM_{10} concentrations from 90 to 200 $\mu g/m^3$. In winter and spring, the potential source areas with the high WPSCF values were distributed in Jiangsu, northern Anhui, Shandong, northeast Henan, eastern Shanxi, southern Hebei, Inner Mongolia, south Mongolia and northeast Xinjiang. These potential source areas contributed $PM_{2.5}$ concentrations from 100 to 180 $\mu g/m^3$ and PM_{10} concentrations from 120 to 180 $\mu g/m^3$. There were clear seasonal and spatial variations of the potential source areas and the airflow in both the horizontal and vertical directions in Beijing. Therefore, more effective regional emission reduction measures in Beijing's surrounding provinces should be designed to reduce the particulate emissions from regional sources in different seasons.

Acknowledgments

This work was supported by the National Key Foundation for Exploring Scientific Instrument (No. 2012YQ060147), the Strategic Priority Research Program of the Chinese Academy of Sciences (No. XDB05040402), and the Key Program of the Chinese 473 Academy of Sciences (No. KJZD-EW-TZ-G06-01).

REFERENCES

Andreae, M.O., Schmid, O., Yang, H., Chand, D., Zhen Yu, J., Zeng, L., et al., 2008. Optical properties and chemical composition of the atmospheric aerosol in urban Guangzhou, China. Atmos. Environ. 42 (25), 6335–6350.

Ashbaugh, L.L., Malm, W.C., Sadeh, W.Z., 1985. A residence time probability analysis of sulfur concentrations at grand Canyon National Park. Atmos. Environ. 19 (8), 1263–1270.

Cao, J.J., Lee, S.C., Ho, K.F., Zou, S.C., Fung, K., Li, Y., et al., 2004. Spatial and seasonal variations of atmospheric organic carbon and elemental carbon in Pearl River Delta Region, China. Atmos. Environ. 38 (27), 4447–4456.

Chen, C., Sun, Y., Xu, W., Du, W., Zhou, L., Han, T., et al., 2015a. Characteristics and sources of submicron aerosols above the

urban canopy (260 m) in Beijing, China, during the 2014 APEC summit. Atmos. Chem. Phys. 15 (22), 12,879–812,895.
Chen, H.S., Li, J., Ge, B.Z., Yang, W.Y., Wang, Z.F., Huang, S., et al., 2015b. Modeling study of source contributions and emergency control effects during a severe haze episode over the Beijing-Tianjin-Hebei area. Sci. China Chem. 58 (9), 1403–1415.
Chen, W., Wang, F.S., Xiao, G.F., Wu, K., Zhang, S.X., 2015c. Air quality of Beijing and impacts of the new ambient air quality standard. Atmosphere-basel 6 (8), 1243–1258.
Gao, J., Tian, H., Cheng, K., Lu, L., Wang, Y., Wu, Y., et al., 2014. Seasonal and spatial variation of trace elements in multi-size airborne particulate matters of Beijing, China: mass concentration, enrichment characteristics, source apportionment, chemical speciation and bioavailability. Atmos. Environ. 99, 257–265.
Guoan, D., Chuenyu, C., Zhiqiu, G., 2005. Vertical structures of PM_{10} and $PM_{2.5}$ and their dynamical character in low atmosphere in Beijing urban area. Sci. China 48 (s2), 38–54.
Han, B., Kong, S.F., Bai, Z.P., Du, G., Bi, T., Li, X., et al., 2010. Characterization of elemental species in $PM_{2.5}$ samples collected in four cities of Northeast China. Water Air Soil Pollut. 209 (1–4), 15–28.
Han, L.H., Cheng, S.Y., Zhuang, G.S., Ning, H.B., Wang, H.Y., Wei, W., et al., 2015. The changes and long-range transport of $PM_{2.5}$ in Beijing in the past decade. Atmos. Environ. 110, 186–195.
Hsu, Y.-K., Holsen, T.M., Hopke, P.K., 2003. Comparison of hybrid receptor models to locate PCB sources in Chicago. Atmos. Environ. 37 (4), 545–562.
Hu, M., Guo, S., Peng, J.F., Wu, Z.J., 2015. Insight into characteristics and sources of $PM_{2.5}$ in the Beijing-Tianjin-Hebei region, China. National Science. Review 2 (3), 257–258.
Jeong, U., Kim, J., Lee, H., Jung, J., Kim, Y.J., Song, C.H., et al., 2011. Estimation of the contributions of long range transported aerosol in East Asia to carbonaceous aerosol and PM concentrations in Seoul, Korea using highly time resolved measurements: a PSCF model approach. J. Environ. Monit. 13 (7), 1905–1918.
Ji, D., Wang, Y., Wang, L., Chen, L., Hu, B., Tang, G., et al., 2012. Analysis of heavy pollution episodes in selected cities of northern China. Atmos. Environ. 50, 338–348.
Karaca, F., Anil, I., Alagha, O., 2009. Long-range potential source contributions of episodic aerosol events to PM_{10} profile of a megacity. Atmos. Environ. 43 (36), 5713–5722.
Katsouyanni, K., Touloumi, G., Samoli, E., Gryparis, A., Le Tertre, A., Monopolis, Y., et al., 2001. Confounding and effect modification in the short-term effects of ambient particles on total mortality: results from 29 European cities within the APHEA2 project. Epidemiology 12 (5), 521–531.
Krewski, D., Burnett, R.T., Goldberg, M.S., Abrahamowicz, M., Siemiatycki, J., Jerrett, M., et al., 2003. Rejoinder: reanalysis of the Harvard Six Cities Study and American Cancer Society study of particulate air pollution and mortality. J. Toxicol. Environ. Health A 66 (16–19), 1715–1722.
Li, L., Wang, Y., Li, J., Xin, L., Jin, J., 2012. The analysis of heavy air pollution in Beijing during 2000–2010. China Environ. Sci. 23–30.
Li, X., Wang, Y., Guo, X., Wang, Y., 2013. Seasonal variation and source apportionment of organic and inorganic compounds in $PM_{2.5}$ and PM_{10} particulates in Beijing, China. J. Environ. Sci. 25 (4), 741–750.
Li, lI., C.JC.-l., Min, Z.H.O.U., 2015a. Potential source contribution analysis of the particulate matters in shanghai during the heavy haze episode in eastern and middle China in December,2013. Environ. Sci. 36 (7), 2327-2236.
Li, J., Xie, S., Zeng, L., Li, L., Li, Y., Wu, R., 2015b. Characterization of ambient volatile organic compounds and their sources in Beijing, before, during, and after Asia-Pacific Economic Cooperation China 2014. Atmos. Chem. Phys. Disc. 15 (8), 12453–12490.
Li, P., Yan, R., Yu, S., Wang, S., Liu, W., Bao, H., 2015c. Reinstate regional transport of $PM_{2.5}$ as a major cause of severe haze in Beijing. Proc. Natl. Acad. Sci. U. S. A. 112 (21), 2739–2740.
Liu, X.G., Sun, K., Qu, Y., Hu, M., Sun, Y.L., Zhang, F., et al., 2015a. Secondary formation of sulfate and nitrate during a haze episode in megacity Beijing, China. Aerosol Air Qual. Res. 15 (6), 2246–2257.
Liu, Z.R., Hu, B., Wang, L.L., Wu, F.K., Gao, W.K., Wang, Y.S., 2015b. Seasonal and diurnal variation in particulate matter (PM_{10} and $PM_{2.5}$) at an urban site of Beijing: analyses from a 9-year study. Environ. Sci. Pollut. R. 22 (1), 627–642.
Lv, B., Liu, Y., Yu, P., Zhang, B., Bai, Y., 2015. Characterizations of $PM_{2.5}$ pollution pathways and sources analysis in four large cities in China. Aerosol Air Qual. Res. 15 (5), 1836–1843.
Meng, R., Zhao, F.R., Sun, K., Zhang, R., Huang, C., Yang, J., 2015. Analysis of the 2014 "APEC blue" in Beijing using more than one decade of satellite observations: lessons learned from radical emission control measures. Remote Sens. 7 (11), 15224–15243.
Menon, S., Hansen, J., Nazarenko, L., Luo, Y., 2002. Climate effects of black carbon aerosols in China and India. Science 297 (5590), 2250–2253.
Polissar, A.V., Hopke, P.K., Harris, J.M., 2001. Source regions for atmospheric aerosol measured at Barrow, Alaska. Environ. Sci. Technol. 35 (21), 4214–4226.
Pope III, C.A., Burnett, R.T., Thun, M.J., Calle, E.E., Krewski, D., Ito, K., et al., 2002. Lung cancer, cardiopulmonary mortality, and long-term exposure to fine particulate air pollution. JAMA-J Am Med Assoc. 287 (9), 1132–1141.
Ren, Z., Wan, B., Su, F., Gao, Q., Zhang, Z., Hong, Z., et al., 2004. Several characteristics of atmospheric environmental quality in China at present. Res. Environ. Sci. 1–6.
Rosenfeld, D., 2000. Suppression of rain and snow by urban and industrial air pollution. Science 287 (5459), 1793–1796.
Simonich, S.L.M., 2009. Response to comments on "atmospheric particulate matter pollution during the 2008 Beijing Olympics". Environ. Sci. Technol. 43 (19), 7590–7591.
Sirois, A., Bottenheim, J.W., 1995. Use of backward trajectories to interpret the 5-year record of pan and O_3 ambient air concentrations at Kejimkujik National Park, Nova Scotia. J. Geophys. Res. 100 (D2), 2867–2881.
Stohl, A., 1996. Trajectory statistics-a new method to establish source-receptor relationships of air pollutants and its application to the transport of particulate sulfate in Europe. Atmos. Environ. 30 (4), 579–587.
Stohl, A., Krompkolb, H., 1994. Origin of ozone in Vienna and surroundings, Austria. Atmos. Environ. 28 (7), 1255–1266.
Streets, D.G., Wu, Y., Chin, M., 2006. Two-decadal aerosol trends as a likely explanation of the global dimming/brightening transition. Geophys. Res. Lett. 33 (15).
Sun, Y., 2012. Reductions of $PM_{2.5}$ in Beijing-Tianjin-Hebei urban agglomerations during the 2008 Olympic Games. Adv. Atmos. Sci. 29 (6), 1330–1342.
Sun, Y., Zhuang, G., Wang, Y., Han, L., Guo, J., Dan, M., et al., 2004. The air-borne particulate pollution in Beijing—concentration, composition, distribution and sources. Atmos. Environ. 38 (35), 5991–6004.
Sun, Y., Song, T., Tang, G.Q., Wang, Y.S., 2013. The vertical distribution of $PM_{2.5}$ and boundary-layer structure during summer haze in Beijing. Atmos. Environ. 74, 413–421.
Sun, K., Liu, X.G., Gu, J.W., Li, Y.P., Qu, Y., An, J.L., et al., 2015. Chemical characterization of size-resolved aerosols in four seasons and hazy days in the megacity Beijing of China. J. Environ. Sci. China 32, 155–167.
Wang, Y.Q., Zhang, X.Y., Arimoto, R., Cao, J.J., Shen, Z.X., 2004. The transport pathways and sources of PM_{10} pollution in Beijing during spring 2001, 2002 and 2003. Geophys. Res. Lett. 31 (14).
Wang, Y.Q., Zhang, X.Y., Arimoto, R., 2006. The contribution from distant dust sources to the atmospheric particulate matter loadings at XiAn, China during spring. Sci. Total Environ. 368 (2–3), 875–883.
Wang, Y.Q., Zhang, X.Y., Draxler, R.R., 2009. TrajStat: GIS-based software that uses various trajectory statistical analysis

methods to identify potential sources from long-term air pollution measurement data. Environ. Model Softw. 24 (8), 938–939.
Wang, Y.Q., Stein, A.F., Draxler, R.R., de la Rosa, J.D., Zhang, X.Y., 2011. Global sand and dust storms in 2008: observation and HYSPLIT model verification. Atmos. Environ. 45 (35), 6368–6381.
Wang, Z.B., Hu, M., Wu, Z.J., Yue, D.L., He, L.Y., Huang, X.F., et al., 2013. Long-term measurements of particle number size distributions and the relationships with air mass history and source apportionment in the summer of Beijing. Atmos. Chem. Phys. 13 (20), 10159–10170.
Wang, W., Maenhaut, W., Yang, W., Liu, X.D., Bai, Z.P., Zhang, T., et al., 2014. One-year aerosol characterization study for $PM_{2.5}$ and PM_{10} in Beijing. Atmos. Pollut. Res. 5 (3), 554–562.
Wang, J.Z., Ho, S.S.H., Cao, J.J., Huang, R.J., Zhou, J.M., Zhao, Y.Z., et al., 2015a. Characteristics and major sources of carbonaceous aerosols in $PM_{2.5}$ from Sanya, China. Sci. Total Environ. 530, 110–119.
Wang, L.L., Liu, Z.R., Sun, Y., Ji, D.S., Wang, Y.S., 2015b. Long-range transport and regional sources of $PM_{2.5}$ in Beijing based on long-term observations from 2005 to 2010. Atmos. Res. 157, 37–48.
Wang, J., Ho, S.S.H., Ma, S., Cao, J., Dai, W., Liu, S., et al., 2016. Characterization of $PM_{2.5}$ in Guangzhou, China: uses of organic markers for supporting source apportionment. Sci. Total Environ. 550, 961–971.
Watson, J.G., 2002. Visibility: science and regulation. J. Air Waste Manage. Assoc. 52 (6), 628–713.
Wehner, B., Birmili, W., Gnauk, T., Wiedensohler, A., 2002. Particle number size distributions in a street canyon and their transformation into the urban-air background: measurements and a simple model study. Atmos. Environ. 36 (13), 2215–2223.
Wei, F., Teng, E., Wu, G., Hu, W., Wilson, W.E., Chapman, R.S., et al., 1999. Ambient concentrations and elemental compositions of PM_{10} and $PM_{2.5}$ in four Chinese cities. Environ. Sci. Technol. 33 (23), 4188–4193.
Xia, X., Chen, H., Zhang, W., 2007. Analysis of the dependence of column-integrated aerosol properties on long-range transport of air masses in Beijing. Atmos. Environ. 41 (36), 7739–7750.
Xin, Y., Wang, G., Chen, L., 2016. Identification of long-range transport pathways and potential sources of PM 10 in Tibetan plateau uplift area: case study of Xining, China in 2014. Aerosol Air Qual. Res. 16 (4), 1044–1054.
Xu, X.H., Barsha, N.A.F., Li, J., 2008. Analyzing regional inluence of particulate matter on the city of Beijing, China. Aerosol Air Qual. Res. 8 (1), 78–93.
Yu, S., Dennis, R.L., Bhave, P.V., Eder, B.K., 2004. Primary and secondary organic aerosols over the United States: estimates on the basis of observed organic carbon (OC) and elemental carbon (EC), and air quality modeled primary OC/EC ratios. Atmos. Environ. 38 (31), 5257–5268.
Yu, S., Alapaty, K., Mathur, R., Pleim, J., Zhang, Y., Nolte, C., et al., 2014a. Attribution of the United States "warming hole": aerosol indirect effect and precipitable water vapor. Sci. Rep-UK. 4, 6929.
Yu, S., Mathur, R., Pleim, J., Wong, D., Gilliam, R., Alapaty, K., et al., 2014b. Aerosol indirect effect on the grid-scale clouds in the two-way coupled WRF–CMAQ: model description, development, evaluation and regional analysis. Atmos. Chem. Phys. 14 (20), 11247–11285.
Zhang, T., Claeys, M., Cachier, H., Dong, S.P., Wang, W., Maenhaut, W., et al., 2008. Identification and estimation of the biomass burning contribution to Beijing aerosol using levoglucosan as a molecular marker. Atmos. Environ. 42 (29), 7013–7021.
Zhang, R., Shen, Z., Cheng, T., Zhang, M., Liu, Y., 2010. The elemental composition of atmospheric particles at Beijing during Asian dust events in spring 2004. Aerosol Air Qual. Res. 10 (1), 67–75.
Zhang, J., Zhu, T., Zhang, Q., Li, C., Shu, H., Ying, Y., et al., 2012. The impact of circulation patterns on regional transport pathways and air quality over Beijing and its surroundings. Atmos. Chem. Phys. 12 (11), 5031–5053.
Zhang, R., Jing, J., Tao, J., Hsu, S.C., Wang, G., Cao, J., et al., 2013. Chemical characterization and source apportionment of $PM_{2.5}$ in Beijing: seasonal perspective. Atmos. Chem. Phys. 13 (14), 7053–7074.
Zhao, X.J., Zhuang, G.S., Wang, Z.F., Sun, Y.L., Wang, Y., Yuan, H., 2007. Variation of sources and mixing mechanism of mineral dust with pollution aerosol - revealed by the two peaks of a super dust storm in Beijing. Atmos. Res. 84 (3), 265–279.
Zhao, X.J., Zhang, X.L., Xu, X.F., Xu, J., Meng, W., Pu, W.W., 2009. Seasonal and diurnal variations of ambient $PM_{2.5}$ concentration in urban and rural environments in Beijing. Atmos. Environment 43 (18), 2893–2900.
Zhao, P., Zhang, X., Xu, X., Zhao, X., 2011a. Long-term visibility trends and characteristics in the region of Beijing, Tianjin, and Hebei, China. Atmos. Res. 101 (3), 711–718.
Zhao, X., Zhang, X., Pu, W., Meng, W., Xu, X., 2011b. Scattering properties of the atmospheric aerosol in Beijing, China. Atmos. Res. 101 (3), 799–808.
Zhao, M.F., Huang, Z.S., Qiao, T., Zhang, Y.K., Xiu, G.L., Yu, J.Z., 2015. Chemical characterization, the transport pathways and potential sources of $PM_{2.5}$ in Shanghai: seasonal variations. Atmos. Res. 158, 66–78.
Zheng, G., Duan, F., Ma, Y., Cheng, Y., Zheng, B., Zhang, Q., et al., 2014. Exploring the severe winter haze in Beijing. Atmos. Chem. Phys. Disc. 14 (12), 17907–17942.
Zhu, L., Huang, X., Shi, H., Cai, X., Song, Y., 2011. Transport pathways and potential sources of PM_{10} in Beijing. Atmos. Environ. 45 (3), 594–604.